Proceedings of the ASME 2015 International Design Engineering Technical Conferences & Computers and Information in Engineering Conference
IDETC/CIE 2015
August 2-5, 2015, Boston, USA

DETC2015/46259

BIFURCATION ANALYSIS OF A SPACECRAFT STRUCTURE USING THE HARMONIC BALANCE METHOD

T. Detroux*, L. Renson, L. Masset, J.P. Noël, G. Kerschen

Space Structures and Systems Laboratory
Aerospace and Mechanical Engineering Department
University of Liège
Liège, Belgium

ABSTRACT

The harmonic balance (HB) method has been widely used in the past few years, as a numerical tool for the study of nonlinear models. However, in its classical formulation the HB method is limited to the approximation of periodic solutions. The present paper proposes to extend the method to the detection and tracking of bifurcations in the codimension-2 system parameters space. To validate the methodology, the forced response of a real spacecraft is examined. The paper first provides some numerical evidence of the presence of quasiperiodic oscillations and isolated solutions. It then demonstrates how the tracking of Neimark-Sacker and fold bifurcations can help get a deeper understanding of these attractors.

1 INTRODUCTION

Because nowadays engineering structures are designed to be lighter and operate in more severe conditions, nonlinear phenomena such as amplitude jumps, modal interactions, limit cycle oscillations and quasiperiodic (QP) oscillations are expected to occur [1]. For most of these nonlinear systems, bifurcations of periodic solutions play a key role in the response dynamics; for example, fold bifurcations indicate a stability change for the solutions, while QP oscillations are encountered in the vicinity of Neimark-Sacker (NS) bifurcations. In that regard, it seems relevant to include stability analysis and bifurcation monitoring while performing parametric studies of the structures.

Time-domain methods such as shooting technique [2] and orthogonal collocation (see, e.g., the MATLAB package MATCONT [3]), which deal with the resolution of a boundary value problem, usually prove accurate to analyze periodic solutions and bifurcations of low-dimensional structures. When applied to larger systems however, their computational burden becomes substantial. As an efficient alternative, most engineers apply a frequency-domain method, the so-called *harmonic balance* (HB) method [4, 5]. Indeed, through the approximation of the solutions with truncated Fourier series, the HB method involves algebraic equations with usually less unknowns than orthogonal collocation. Nevertheless, in spite of its performance and accuracy, the HB method has never been extended to track bifurcations of mechanical structures. This is why the present paper proposes an extension of the methodology to study bifurcations in the system parameters space.

The first part of this paper is devoted to the HB theory and its formulation in the framework of a continuation algorithm for bifurcation tracking. In section 3, the methodology is validated with the analysis of the nonlinear dynamics of a spacecraft.

*Address all correspondence to this author, email: tdetroux@ulg.ac.be.

2 HARMONIC BALANCE METHOD FOR BIFURCATION ANALYSIS

2.1 Formulation of the dynamics in the frequency domain

This section first performs a brief review of the theory of the HB procedure. The method will be applied to general non-autonomous nonlinear dynamical systems with n degrees of freedom (DOFs) whose equations of motion are

$$\mathbf{M}\ddot{\mathbf{x}} + \mathbf{C}\dot{\mathbf{x}} + \mathbf{K}\mathbf{x} = \mathbf{f}_{ext}(\omega, t) - \mathbf{f}_{nl}(\mathbf{x}, \dot{\mathbf{x}}) = \mathbf{f}(\mathbf{x}, \dot{\mathbf{x}}, \omega, t) \quad (1)$$

where $\mathbf{M}$, $\mathbf{C}$ and $\mathbf{K}$ are the mass, damping and stiffness matrices respectively, $\mathbf{x}$ represents the displacements, the dots refer to the derivatives with respect to time t, $\mathbf{f}_{nl}$ represents the nonlinear forces and $\mathbf{f}_{ext}$ stands for the periodic external forces (harmonic excitation, for example) with frequency ω. The term $\mathbf{f}$ gathers both the external and nonlinear forces.

As recalled in the introduction, the periodic solutions $\mathbf{x}(t)$ and $\mathbf{f}(t)$ of equation (1) are approximated by Fourier series truncated to the N_H-th harmonic:

$$\mathbf{x}(t) = \frac{\mathbf{c}_0^x}{\sqrt{2}} + \sum_{k=1}^{N_H} \left(\mathbf{s}_k^x \sin\left(\frac{k\omega t}{\nu}\right) + \mathbf{c}_k^x \cos\left(\frac{k\omega t}{\nu}\right) \right) \quad (2)$$

$$\mathbf{f}(t) = \frac{\mathbf{c}_0^f}{\sqrt{2}} + \sum_{k=1}^{N_H} \left(\mathbf{s}_k^f \sin\left(\frac{k\omega t}{\nu}\right) + \mathbf{c}_k^f \cos\left(\frac{k\omega t}{\nu}\right) \right) \quad (3)$$

where $\mathbf{s}_k$ and $\mathbf{c}_k$ represent the $n \times 1$ vectors of Fourier coefficients related to the sine and cosine terms, respectively. Here it is interesting to note that the Fourier coefficients of $\mathbf{f}(t)$, $\mathbf{c}_k^f$ and $\mathbf{s}_k^f$, depend on the Fourier coefficients of the displacements $\mathbf{x}(t)$, $\mathbf{c}_k^x$ and $\mathbf{s}_k^x$. The integer parameter ν is introduced to account for some possible subharmonics of the external excitation frequency ω.

Substituting expressions (3) in equations (1) and balancing the harmonic terms with a Galerkin projection yields the following nonlinear equations in the frequency domain (see [6] for further details)

$$\mathbf{h}(\mathbf{z}, \omega) \equiv \mathbf{A}(\omega)\mathbf{z} - \mathbf{b}(\mathbf{z}) = \mathbf{0} \quad (4)$$

where $\mathbf{A}$ is the $(2N_H+1)n \times (2N_H+1)n$ matrix describing the linear dynamics of the system, $\mathbf{z}$ is the vector containing all the Fourier coefficients of the displacements $\mathbf{x}(t)$, and $\mathbf{b}$ represents the vector of the Fourier coefficients of the external and nonlinear forces $\mathbf{f}(t)$. They have the following expressions:

$$\mathbf{A} = \begin{bmatrix} \mathbf{K} & & & \\ & \tilde{\mathbf{K}}_1 & & \\ & & \ddots & \\ & & & \tilde{\mathbf{K}}_{N_H} \end{bmatrix} \quad (5)$$

$$\tilde{\mathbf{K}}_i = \begin{bmatrix} \mathbf{K} - \left(\frac{i\omega}{\nu}\right)^2 \mathbf{M} & -\frac{i\omega}{\nu}\mathbf{C} \\ \frac{i\omega}{\nu}\mathbf{C} & \mathbf{K} - \left(\frac{i\omega}{\nu}\right)^2 \mathbf{M} \end{bmatrix} \quad (6)$$

$$\mathbf{z} = \begin{bmatrix} \left(\mathbf{c}_0^x\right)^T & \left(\mathbf{s}_1^x\right)^T & \left(\mathbf{c}_1^x\right)^T & \dots & \left(\mathbf{s}_{N_H}^x\right)^T & \left(\mathbf{c}_{N_H}^x\right)^T \end{bmatrix}^T \quad (7)$$

$$\mathbf{b} = \begin{bmatrix} \left(\mathbf{c}_0^f\right)^T & \left(\mathbf{s}_1^f\right)^T & \left(\mathbf{c}_1^f\right)^T & \dots & \left(\mathbf{s}_{N_H}^f\right)^T & \left(\mathbf{c}_{N_H}^f\right)^T \end{bmatrix}^T \quad (8)$$

In the time domain, expression (1) contains n equations while, in the frequency domain, expression (4) has $(2N_H+1)n$ unknowns gathered in $\mathbf{z}$. Expression (4) can be seen as the equations of amplitude of (1): if $\mathbf{z}^*$ is a root of (4), then the time signals $\mathbf{x}^*$ constructed from $\mathbf{z}^*$ with (3) are solutions of the equations of motion (1) and are periodic. When embedded in a continuation procedure, solutions of (4) can be tracked with respect to the frequency ω, which gives a frequency response of the system.

2.2 Stability analysis and detection of bifurcations

In the frequency domain, the stability of a periodic solution is usually assessed with Hill's method, which provides approximation of the Floquet exponents. In [7], it is shown that these exponents, here denoted $\tilde{\lambda}$, can be found as the eigenvalues of a matrix $\tilde{\mathbf{B}}$. The components of this matrix are by-products of the HB method, i.e., depend only on $\mathbf{M}$, $\mathbf{C}$, $\mathbf{K}$ and $\mathbf{J}_z$, the jacobian of (4) with respect to $\mathbf{z}$. If at least one of the Floquet exponents has a positive real part, then the solution is unstable, otherwise it is asymptotically stable.

In this work, the detection of fold (F) and NS bifurcations along the frequency response is sought. This is achieved through the evaluation of test functions at each iteration of the branch, which have the property to pass through zero at a bifurcation. From the Floquet theory, it is known that a fold bifurcation is detected when one of the Floquet exponents $\tilde{\lambda}$ crosses the imaginary axis through the real axis. As a consequence, the following test function has a root at a fold bifurcation:

$$\phi_F = \left|\tilde{\mathbf{B}}\right| \quad (9)$$

The NS bifurcations are characterized by a pair of Floquet exponents crossing the imaginary axis as complex conjugates. A dedicated test function is thus

$$\phi_{NS} = \left|\tilde{\mathbf{B}}_{\odot}\right| \tag{10}$$

where $\tilde{\mathbf{B}}_{\odot}$ stands for the bialternate matrix product of $\tilde{\mathbf{B}}$, which has the property to be singular when $\tilde{\mathbf{B}}$ has two complex-conjugate eigenvalues with no real part.

2.3 Tracking of bifurcations

In order to track bifurcations in a codimension-2 parameter space, one has to append one equation to (4), describing the bifurcation of interest:

$$\begin{cases} \mathbf{h} = 0 \\ \phi = 0 \end{cases} \tag{11}$$

Instead of considering $\phi = \phi_F$ and $\phi = \phi_{NS}$, which can lead to scaling problems for large matrices, in this paper the use of the so-called *bordering technique* [8] is proposed. The idea behind this technique is to replace the evaluation of the determinant of a given matrix $\mathbf{G}$ by the evaluation of a scalar function, herein denoted g, which vanishes as regular zero for the same system state and parameters as the determinant. It can be shown that a candidate for g is obtained by solving the bordered system

$$\begin{bmatrix} \mathbf{G} & \mathbf{p} \\ \mathbf{q}^* & 0 \end{bmatrix} \begin{bmatrix} \mathbf{w} \\ g \end{bmatrix} = \begin{bmatrix} \mathbf{0} \\ 1 \end{bmatrix} \tag{12}$$

In this system, * denotes a conjugate transpose, and vectors $\mathbf{p}$ and $\mathbf{q}$ are chosen to ensure the nonsingularity of the bordered matrix. From (9-10), one then proposes the following equations for the extended system (11):

$$\text{Fold bifurcations:} \quad \phi = g_F \quad \text{with} \quad \mathbf{G}_F = \tilde{\mathbf{B}} \tag{13}$$

$$\text{NS bifurcations:} \quad \phi = g_{NS} \quad \text{with} \quad \mathbf{G}_{NS} = \tilde{\mathbf{B}}_{\odot} \tag{14}$$

Besides its numerical efficiency for large systems, the bordering technique has interesting features regarding its implementation in a continuation procedure. Indeed, analytical expressions can be obtained for the derivatives of g with respect to $\mathbf{z}$ and to the parameters of the system [8]. This requires the eigenvalues derivatives of $\tilde{\mathbf{B}}$, that are explicitly evaluated using the method proposed in [9].

3 VALIDATION OF THE METHOD ON AN INDUSTRIAL STRUCTURE WITH STRONG NONLINEARITIES

In this section, the HB method is used to address the continuation of periodic solutions of a large-scale structure, and the detection and tracking of their bifurcations.

3.1 Case study: SmallSat spacecraft

The example studied is referred to as the *SmallSat*, a structure represented in Figure 1(a) and which was conceived by EADS-Astrium as a platform for small satellites. The interface between the spacecraft and launch vehicle is achieved via four aluminum brackets located around cut-outs at the base of the structure. The total mass of the spacecraft including the interface brackets is around 64 kg, it is 1.2 m in height and 1 m in width. It supports a dummy telescope mounted on a baseplate through a tripod, and the telescope plate is connected to the SmallSat top floor by three shock attenuators, termed *shock attenuation systems for spacecraft and adaptor* (SASSAs), whose dynamical behavior may exhibit nonlinearity.

Besides, as depicted in Figure 1(b), a support bracket connects to one of the eight walls the so-called *wheel elastomer mounting system* (WEMS) device which is loaded with an 8-kg dummy inertia wheel. The WEMS device is a mechanical filter which mitigates disturbances coming from the inertia wheel through the presence of a soft elastomeric interface between its mobile part, i.e. the inertia wheel and a supporting metallic cross, and its fixed part, i.e. the bracket and by extension the spacecraft. Moreover, eight mechanical stops limit the axial and lateral motions of the WEMS mobile part during launch, which gives rise to strongly nonlinear dynamical phenomena. A thin layer of elastomer placed onto the stops is used to prevent metal-metal impacts. Figure 1(c) presents a simplified though relevant modeling of the WEMS device where the inertia wheel, owing to its important rigidity, is seen as a point mass. The four nonlinear connections (NCs) between the WEMS mobile and fixed parts are labeled NC1 – 4. Each NC possesses a trilinear spring in the axial direction (elastomer in traction/compression plus two stops), a bilinear spring in the radial direction (elastomer in shear plus one stop) and a linear spring in the third direction (elastomer in shear). In Figure 1(c), linear and nonlinear springs are denoted by squares and circles, respectively.

A finite element model (FEM) of the SmallSat was developed and used in the present work to conduct numerical experiments. It comprises about 150,000 DOFs and the comparison with experimental data revealed its good predictive capabilities.

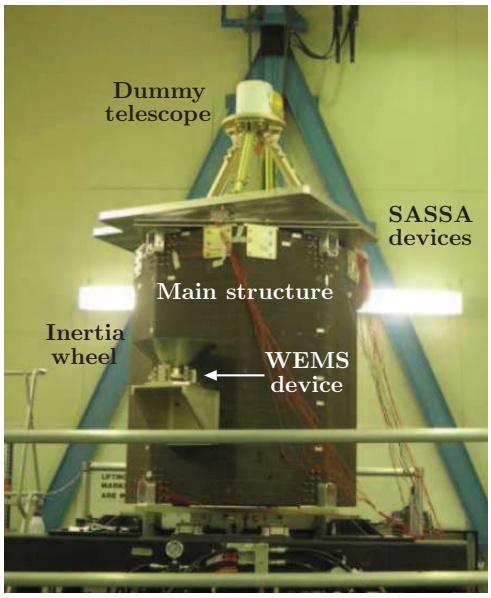

(a)

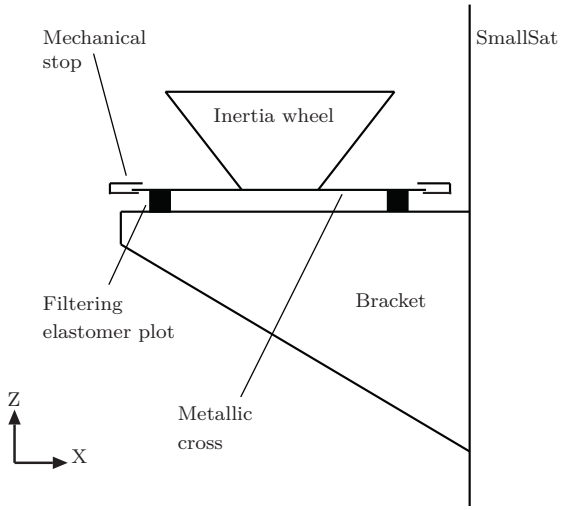

(b)

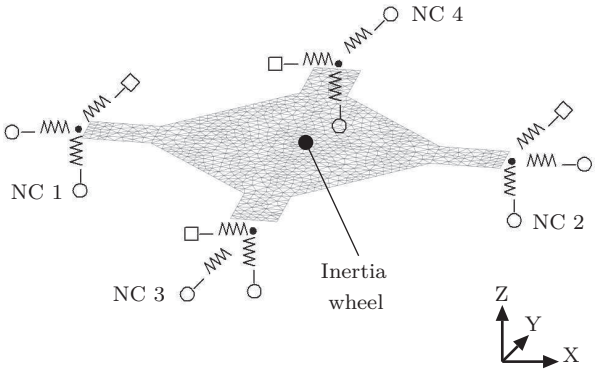

(c)

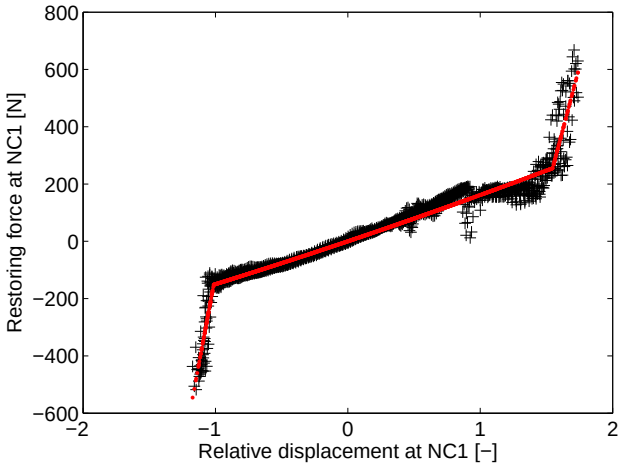

(d)

FIGURE 1: SmallSat spacecraft equipped with an inertia wheel supported by the WEMS and a dummy telescope connected to the main structure by the SASSA isolators. (a) Photograph. (b) Schematic of the nonlinear vibration isolation device. (c) Simplified modeling of the WEMS mobile part considering the inertia wheel as a point mass. The linear and nonlinear connections between the WEMS mobile and fixed parts are signaled by squares and circles, respectively. (d) Experimental stiffness curve of NC1 constructed using the restoring force surface method (in black) and fitted with a trilinear model (in red).

The model consists of shell elements (octagon structure and top floor, instrument baseplate, bracket and WEMS metallic cross) and point masses (dummy inertia wheel and telescope) and meets boundary conditions with four clamped nodes. Proportional damping is considered and the high dissipation in the elastomer components of the WEMS is described using lumped dashpots with coefficients $c_{ax} = 63\,\text{Ns/m}$ and $c_{lat} = 37\,\text{Ns/m}$ for axial (vertical) and lateral directions, respectively; this results in a highly non-proportional damping matrix. Then, to achieve tractable nonlinear calculations, the linear elements of the FEM were condensed using the Craig-Bampton reduction technique. This approach consists in expressing the system dynamics in terms of some retained DOFs and internal modes of vibration. Specifically, the full-scale model of the spacecraft was reduced to 9 nodes (excluding DOFs in rotation), namely both sides of each NC and the vertical DOF of the inertia wheel, with 10 internal modes. In total, the reduced-order model thus contains 37 DOFs. Bilinear and trilinear springs were finally introduced within the WEMS module between the NC nodes to model the nonlinearities of the connections between the WEMS and the rest of the SmallSat. To avoid numerical issues, regularization with third-order polynomials was utilized in the close vicinity of the clearances to implement C^1 continuity. The WEMS nonlinearities are the only nonlinear components introduced in the model. They were accurately identified in [10] using measured data from swept-sine base excitations at different amplitude levels. For instance, the stiffness curve characterizing NC1, identified using the restoring force surface method [11], is depicted in Figure 1(d). For confidentiality, clearances and displacements of the SmallSat are given through adimensionalised quantities throughout the paper.

3.2 Nonlinear dynamics and bifurcations of the SmallSat

The first part of the study is carried out around the 6th mode of the SmallSat, which corresponds to a linear frequency of 28.75 Hz. However, it was shown by Renson *et al.* [12] that this nonlinear mode undergoes a substantial increase in frequency due to the frequency-energy dependence of the structure. The HB method highlighted in this paper is applied to compute the forced response of the structure for vertical excitations on the DOF of the inertia wheel, in this frequency range of interest.

Figure 2(a) depicts the system's frequency response curve computed with $N_H = 9$ harmonics retained in the Fourier approximation and $N = 1024$ points per period. For this result and others in the paper, no subharmonic solution is sought ($\nu = 1$). The amplitude of the periodic solutions computed is represented, that is the maximum displacement of the DOF of interest along the period. The evolution of the normalized harmonic coefficients σ_i ($i = 1,\ldots,N_H$) for this DOF along the branch is given in Figure 2(b), where the harmonic coefficients are constructed as

$$\begin{aligned} \rho_0 &= \frac{c_0^x}{\sqrt{2}} \\ \rho_i &= \sqrt{(s_i^x)^2 + (c_i^x)^2} \quad (i = 1,\ldots,N_H) \end{aligned} \tag{15}$$

and where the following normalization applies:

$$\sigma_i = \frac{\rho_i}{\sum_{k=0}^{N_H} \rho_i} \quad (i = 0,\ldots,N_H) \tag{16}$$

From 20 to 23 Hz, only the fundamental frequency is present in the response. When the excitation enters the resonance region, the nonlinearities of the SmallSat activate other harmonics in the response such as the second and third ones. Even harmonics have a contribution in the dynamics because of the asymmetrical modeling of the connections with the WEMS. From the figure, it is also clear that the 6th and higher harmonics have a negligible participation to the response; for this reason, a number of harmonics $N_H = 5$ retained in the Fourier series is considered throughout the rest of the paper. It is also possible to demonstrate that the number of $N = 1024$ points per period is sufficient to capture the dynamics in play.

Circle and triangle markers denote the fold and NS bifurcations, respectively, that are detected along the branch in Figure 2(a), and the stability of the solutions is also given. One observes that a pair of fold bifurcations is present in the bending segments of the resonance peak, which is due to the hardening behavior of the system, and which gives rise to a change in stability of the periodic solutions. One also notices a pair of NS bifurcations, which means that stable quasiperiodic solutions could be found in their vicinity.

As a verification, the frequency response computed with HB method is superimposed to a swept-sine response computed with a Newmark integration scheme, in Figure 3(a), for a forcing amplitude $F = 155\,\text{N}$. For this swept-sine excitation, the applied sweep rate is 0.5 Hz/min and the sampling frequency is 3000 Hz. Along with the fact that the frequency response provides accurate estimation of the displacement envelope, as expected, one also notes that the bifurcations are directly related to the nonlinear phenomena observed. On the one hand, a fold bifurcation accurately points out the location of a jump from high to low amplitude. On the other hand, unexpected large oscillations are observed in Figure 3(a), and are created and eliminated at the first and second NS bifurcations, respectively.

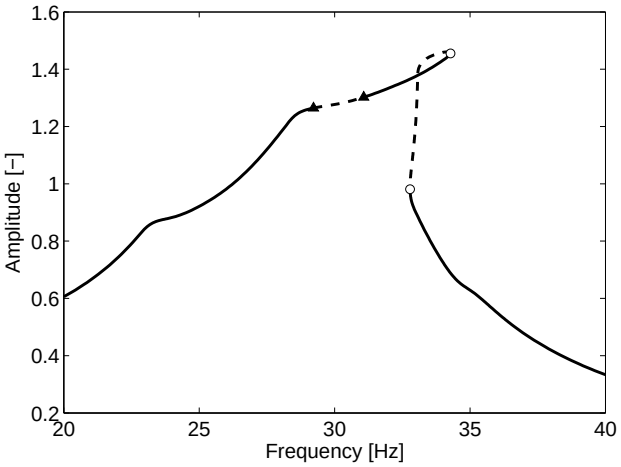

(a)

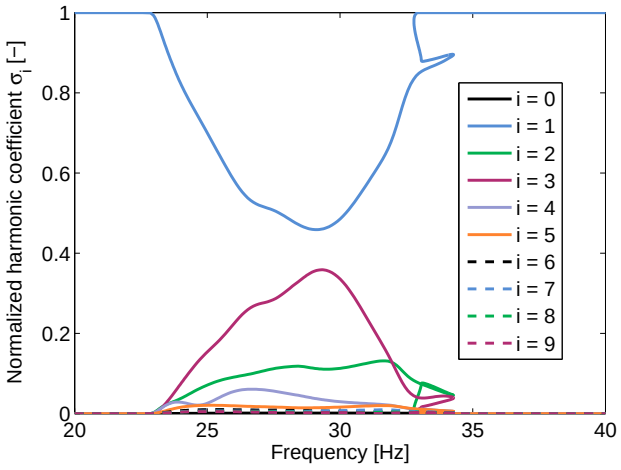

(b)

FIGURE 2: SmallSat frequency response at NC1-Z node for harmonic excitations of amplitude $F = 155\,\mathrm{N}$ applied to the inertia wheel, obtained with the HB method ($N_H = 9$ and $N = 1024$). (a) Displacement responses with circle and triangle markers depicting fold and NS bifurcations, respectively. The solid and dashed lines represent stable and unstable solutions, respectively. (b) Harmonic coefficients responses.

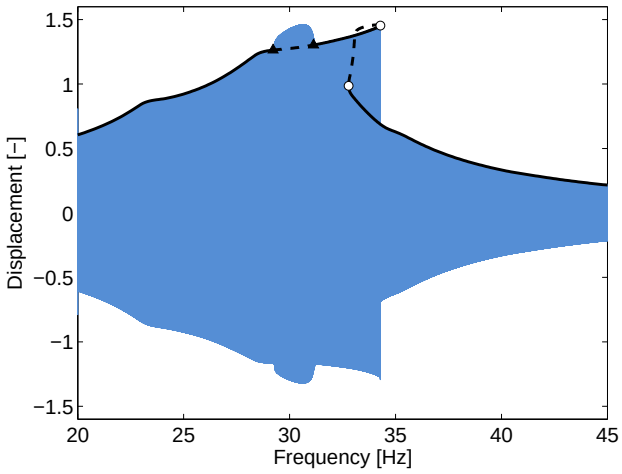

(a)

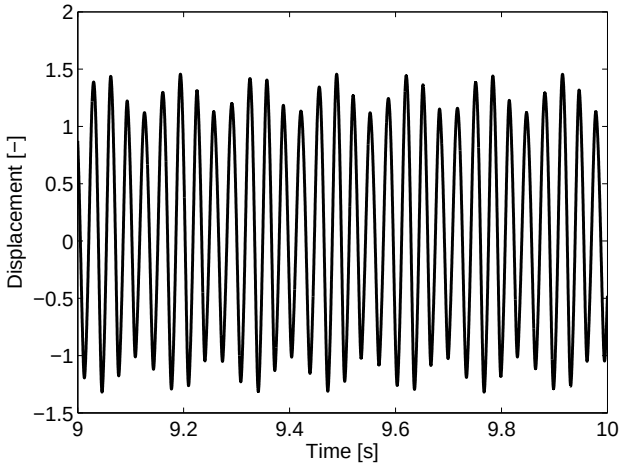

(b)

FIGURE 3: Comparison between the HB method ($N_H = 5$ and $N = 1024$) and a Newmark time integration scheme, for excitations of amplitude $F = 155\,\mathrm{N}$ applied to the inertia wheel. (a) SmallSat displacement response at NC1-Z node. Swept-sine response obtained from time simulation with a sampling frequency of 3000 Hz (blue line), and frequency responses obtained with the HB method (black line). Circle and triangle markers depict fold and NS bifurcations, respectively. The solid and dashed lines represent stable and unstable solutions, respectively. (b) Time response of the NC1-Z node of the SmallSat for a harmonic excitation of frequency $\omega = 30.5\,\mathrm{Hz}$.

A time response of the system to a single harmonic excitation of forcing amplitude $F = 155\,\text{N}$ and frequency $\omega = 30.5\,\text{Hz}$ is provided in Figure 3(b), i.e. in the frequency interval of the unexpected resonance. One observes that quasiperiodic oscillations occur for this operation regime, which is explained by the presence of the two NS bifurcations. In this case, their importance has to be carefully assessed since they have amplitude as large as that of the resonance.

3.3 Influence of the forcing amplitude F and the axial damping c_{ax} on the fold and NS bifurcations

The purpose of this section is to validate the HB methodology for the tracking of bifurcations. To this end, a tracking of the fold bifurcations in the codimension-2 forcing frequency-ω and amplitude-F space is first performed using the outlined technique. Figure 4(a) represents the fold curve obtained, together with the frequency responses of the system for different forcing levels. Figure 4(b) also shows the projection of this curve in the F-amplitude plane. Very interestingly, the fold branch first tracks the bifurcations of the main frequency response, and then turns back to reveal *detached resonance curves* (DRC), or *isolas*, that are rarely observed for such large systems [13, 14]. These DRCs are created around the resonance peak at a forcing amplitude $F = 158\,\text{N}$, then expands both in frequency and amplitude, until one reaches a forcing amplitude $F = 170\,\text{N}$ at which they merge with this resonance peak. It can be shown that the upper part of the DRCs is stable; as a direct consequence, the merging of the DRC with the resonance peak leads to a sudden increase of the latter in frequency and amplitude.

Focusing now on NS bifurcations, one can also study the effect of a design parameter of the system such as c_{ax} on the quasiperiodic oscillations. Figure 5(a) depicts the evolution of the NS curve in the codimension-2 forcing frequency-ω and axial damping c_{ax} space, to which one superimposes frequency responses computed for $c_{ax} = 63\,\text{Ns/m}$, $80\,\text{Ns/m}$ and $85\,\text{Ns/m}$. Its projection in the c_{ax}-amplitude plane is also given in Figure 5(b). It is interesting to note that increasing the axial damping up to a value of $84\,\text{Ns/m}$ eliminates the NS bifurcations, while it does not significantly affect the resonance peaks.

The convergence properties of the bifurcation tracking is assessed in Figure 6, for which the fold and NS curves presented in Figures 4 and 5 were recomputed for different number of harmonics N_H, from 1 to 9. As a result, Figure 6(a) shows the influence of N_H on the forcing amplitudes at which the DRC is created and merges with the main frequency response, with the diamond and square markers, respectively. Similarly, Figure 6(b) represents the influence of N_H on the axial damping c_{ax} at which the NS are eliminated on the NS curve. For both figures, the convergence of the forcing amplitude and axial damping is verified. While the convergence is monotonic for the fold curves, it has no clear trend for the NS curves. As concluded above in Figure 2(b), a number of 5 harmonics retained in the Fourier series gives an acceptable approximation since the convergence curve remains bounded in a 1%-error interval.

4 CONCLUSIONS

The purpose of this paper was twofold. First, it intended to extend the harmonic balance method from the computation of periodic solutions to the tracking of their bifurcations in codimension-2 parameter space. To this end, Hill's method and bordering techniques were combined and embedded in a continuation procedure in order to obtain a robust and efficient algorithm able to deal with large engineering structures.

In the second part of this paper, the HB method and its extension were applied to the SmallSat spacecraft, an industrial and complex model with several localized nonlinearities. The computation of the frequency response and the detection of its bifurcation were performed, which indicated the presence of NS and fold bifurcations. A swept-sine excitation study on the structure showed that high amplitude quasiperiodic oscillations emanate from the NS bifurcations. The tracking of fold bifurcations then highlighted the presence of detached resonance curves, which is rarely discussed in the technical literature. Together with the explanations about the SmallSat dynamics they provide, these results demonstrate that crucial information can be missed when one only performs continuation of periodic solutions. Obviously, a tracking in codimension-2 space is necessary in order to reveal detached resonance curves. It also proves useful for the design of some components of the structure, if a reduction of the quasiperiodic oscillations is sought.

ACKNOWLEDGEMENTS

The authors Thibaut Detroux, Luc Masset and Gaetan Kerschen would like to acknowledge the financial support of the European Union (ERC Starting Grant NoVib 307265). The author L. Renson is a Marie-Curie COFUND Postdoctoral Fellow of the University of Liège, co-funded by the European Union. The author J.P. Noël is a Postdoctoral Researcher of the *Fonds de la Recherche Scientifique FNRS* which is gratefully acknowledged.

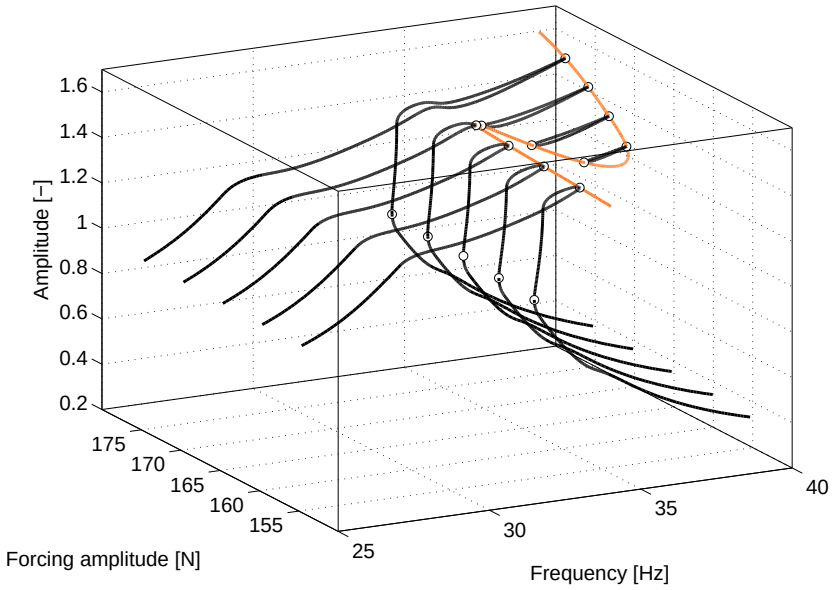

(a)

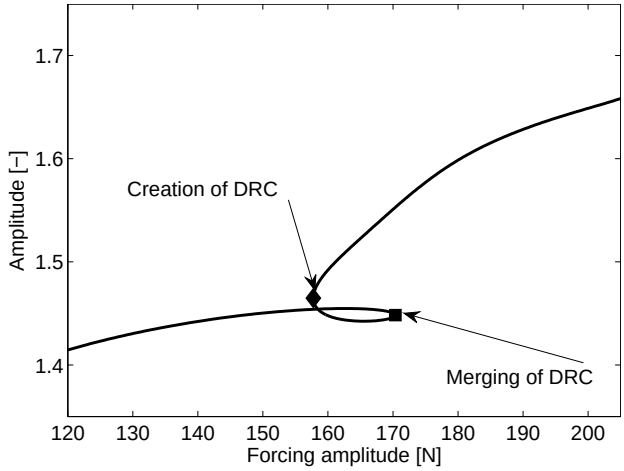

(b)

FIGURE 4: Merging of the detached resonance curve with the main frequency response. (a) The orange line represents the branch of fold bifurcations tracked with respect to the excitation amplitude F and frequency ω. Frequency responses of the NC1-Z node for harmonic excitations of amplitude $F = 155\,\text{N}$, $160\,\text{N}$, $170\,\text{N}$ and $175\,\text{N}$ are also given with the black lines. The axial damping value is fixed at $c_{ax} = 63\,\text{Ns/m}$. Circle markers depict fold bifurcations. (b) Projection of the branch of fold bifurcations on the F-amplitude plane. The forcing amplitudes at which the DRC is created and merges with the main frequency response are signaled with diamond and square markers, respectively.

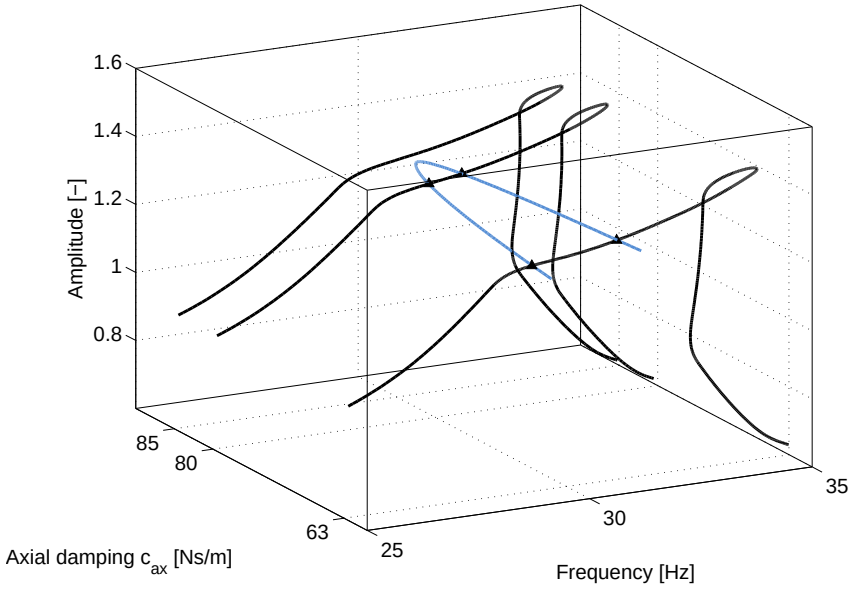

(a)

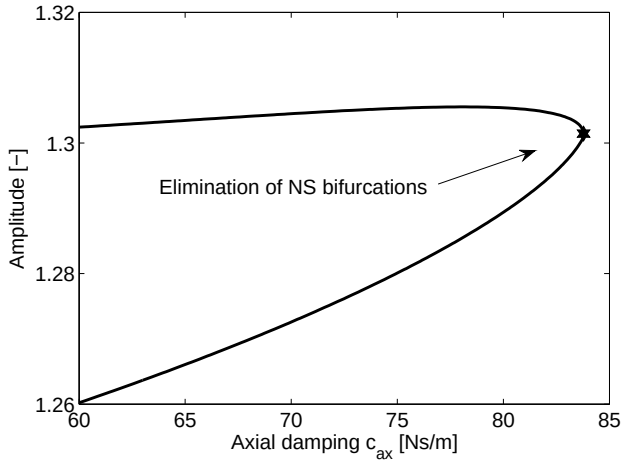

(b)

FIGURE 5: Elimination of the NS bifurcations. (a) The blue line represents the branch of NS bifurcations tracked with respect to the axial damping coefficient c_{ax} and frequency ω. Frequency responses of the NC1-Z node for harmonic excitations of amplitude $F = 155\,\mathrm{N}$, and for configurations with $c_{ax} = 63\,\mathrm{Ns/m}$ (reference), $80\,\mathrm{Ns/m}$ and $85\,\mathrm{Ns/m}$ are also given with the black lines. Triangle markers depict NS bifurcations. (b) Projection of the branch of NS bifurcations on the c_{ax}-amplitude plane. The axial damping value at which the NS bifurcations are eliminated is signaled with the star marker.

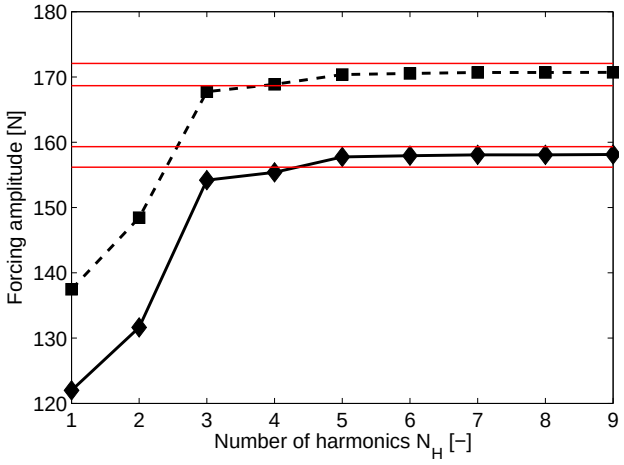

(a)

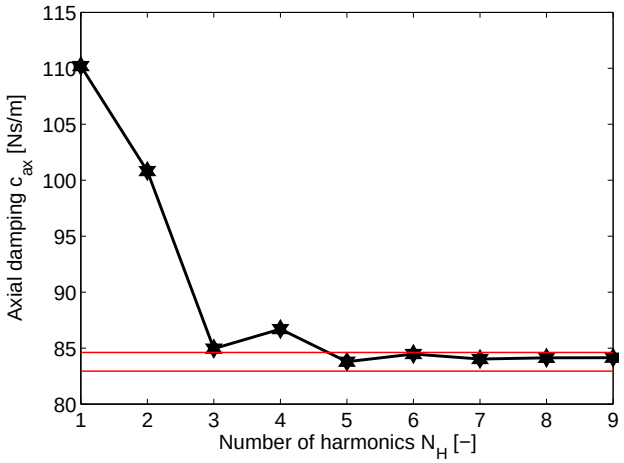

(b)

FIGURE 6: Convergence study of the bifurcation tracking with respect to the number of harmonics N_H. (a) Evolution of the forcing amplitudes at which the DRC is created (solid line and diamond markers), and at which it merges with the main frequency response (dashed line and square markers). The axial damping is kept constant, with $c_{ax} = 63\,\text{Ns/m}$. (b) The solid line and stars markers represent the axial damping c_{ax} at which the NS bifurcations are eliminated. The forcing amplitude is kept constant, with $f = 155\,\text{N}$. For both figures, the red lines gives $+1\%$ and -1% variations of the value related to $N_H = 5$.

REFERENCES

[1] Nayfeh, A. H., and Mook, D. T., 2008. *Nonlinear oscillations*. John Wiley & Sons.

[2] Peeters, M., Viguié, R., Sérandour, G., Kerschen, G., and Golinval, J.-C., 2009. "Nonlinear normal modes, Part II: Toward a practical computation using numerical continuation techniques". *Mechanical Systems and Signal Processing*, ***23***(1), pp. 195–216.

[3] Dhooge, A., Govaerts, W., and Kuznetsov, Y. A., 2003. "Matcont: a matlab package for numerical bifurcation analysis of odes". *ACM Transactions on Mathematical Software (TOMS)*, ***29***(2), pp. 141–164.

[4] Cardona, A., Coune, T., Lerusse, A., and Geradin, M., 1994. "A multiharmonic method for non-linear vibration analysis". *International Journal for Numerical Methods in Engineering*, ***37***(9), pp. 1593–1608.

[5] von Groll, G., and Ewins, D. J., 2001. "The harmonic balance method with arc-length continuation in rotor/stator contact problems". *Journal of Sound and Vibration*, ***241***(2), pp. 223–233.

[6] Jaumouillé, V., Sinou, J.-J., and Petitjean, B., 2010. "An adaptive harmonic balance method for predicting the nonlinear dynamic responses of mechanical systems - Application to bolted structures". *Journal of Sound and Vibration*, ***329***(19), pp. 4048–4067.

[7] Detroux, T., Renson, L., and Kerschen, G., 2014. "The harmonic balance method for advanced analysis and design of nonlinear mechanical systems". In Proceedings of the 32th International Modal Analysis Conference (IMAC).

[8] Govaerts, W. J., 2000. *Numerical methods for bifurcations of dynamical equilibria*, Vol. 66. SIAM.

[9] Van Der Aa, N., Ter Morsche, H., and Mattheij, R., 2007. "Computation of eigenvalue and eigenvector derivatives for a general complex-valued eigensystem". *Electronic Journal of Linear Algebra*, ***16***(1), pp. 300–314.

[10] Noël, J., Renson, L., and Kerschen, G., 2014. "Complex dynamics of a nonlinear aerospace structure: Experimental identification and modal interactions". *Journal of Sound and Vibration*, ***333***(12), pp. 2588–2607.

[11] Masri, S., and Caughey, T., 1979. "A nonparametric identification technique for nonlinear dynamic problems". *Journal of Applied Mechanics*, ***46***(2), pp. 433–447.

[12] Renson, L., Noël, J., and Kerschen, G., 2015. "Complex dynamics of a nonlinear aerospace structure: numerical continuation and normal modes". *Nonlinear Dynamics*, ***79***(2), pp. 1293–1309.

[13] Takács, D., Stépán, G., and Hogan, S. J., 2008. "Isolated large amplitude periodic motions of towed rigid wheels". *Nonlinear Dynamics*, ***52***(1-2), pp. 27–34.

[14] Alexander, N. A., and Schilder, F., 2009. "Exploring the performance of a nonlinear tuned mass damper". *Journal of Sound and Vibration*, ***319***(1), pp. 445–462.